Imperial College London

KINEXUS

Attitude Determination System Design for Asteroid Redirect Mission

Rohin Nayar
CID: 01844054
ARM04 Spacecraft Subsystem Design Team

Academic Supervisors:	Thulasi Mylvaganam & Roderick Lubbock
Department:	Department of Aeronautics
Course:	MEng Aeronautical Engineering
Module:	AERO 60004
Academic Year:	2022/2023
Date:	December 21, 2023

Department of Aeronautics
South Kensington Campus
Imperial College London
London SW7 2AZ
U.K.

Abstract

The attitude determination system for the *Kinexus* spacecraft, an asteroid kinetic impactor vehicle, has been designed. This report outlines the system design, which aims to provide a highly accurate state estimator algorithm to achieve stringent fine-pointing accuracy requirements. The proposed system includes quantifying the disturbance environment, selecting appropriate sensor hardware, implementing redundancy architecture, and evaluating various attitude determination algorithms. By comparing the Root Mean Square Error (RMSE), it was determined that the Unscented Kalman Filter (UKF) exhibited the best performance in the spacecraft simulation scenario. Subsequent Monte Carlo simulations were conducted to optimize the characteristic parameters. As a result, a robust dual attitude determination algorithm was developed by combining the Quaternion Estimator (QUEST) algorithm with the UKF. This integrated approach is presented to deliver precise state estimation and effectively address attitude drift challenges associated with deep space spacecraft attitude control.

Keywords: Attitude Determination, Sensor Hardware, Unscented Kalman Filter, Quaternion Estimator, Monte Carlo simulations

ARM23: Project Kinexus		
Subteam	**Members**	**CID**
Project Coordination	Bashshar Khan	01728050
	Ridge Falcao	01930859
	Zayd Islam	01864154
Mission Design and Analysis	Alexander Hook	01849196
	Gil Barbosa Ribeiro	01927634
	Kiryl Tarasenka	01857233
	Piotr Fil	01863515
Spacecraft Mechanical Design and Subsystem Integration	Aaron Patel	01858148
	Alexis Renaud	01933904
	Arun Herai	01846724
	Jayden Ting	01843064
	Joshua Long	01858013
	Paula Alvarez Solanas	01874174
Spacecraft Subsystem Design	Aryaa Desai	01846886
	Benjamin Frisch	02356928
	Dian Westerhoven	01861214
	Louis Christodoulou	01735370
	Martin Aurelius Widojo	01873070
	Rohin Nayar	**01844054**
	Sachin Solanki	01845905
	Owen Brook	01853696
Asteroid Re-direction Trajectory Analysis	Gabriel Kotovsky	01861913
	Pantelis Koshias	01744262
	Yan Taylor Pan	01856795
Launch Vehicle and Ground Systems	Antonios Iannou-Skenter	01929659
	Junglin Sung	01725815
	Karel Coetzee	01873898
	Stanislas Chavel	01907423

Contents

List of Figures

List of Tables

List of Symbols

a	Scalar quantity	$\bar{\mathbf{A}}_{\text{bias}}$	Bias acceleration vector
$\bar{\mathbf{A}}_{\text{imeas}}$	Acceleration measured	$\bar{\mathbf{A}}_{\text{meas}}$	Measured acceleration vector
$\bar{\mathbf{A}}_{\text{SF}}$	Scale factor Acceleration vector	$\bar{P}^{+}$	State estimate covariance
A_{s}	Surface area exposed to the sun	c	Speed of light
$\boldsymbol{\chi}_k(i)$	Sigma Point Matrix	$\boldsymbol{\delta}\bar{\mathbf{q}}(\mathbf{a})$	Quaternion Error
$\dot{\mathbf{g}}$	Time derivative of Gibbs vector	$\hat{\boldsymbol{s}}_b$	Unit sun vector in body frame
$\hat{\boldsymbol{s}}_i$	Unit sun vector in inertial frame	$\hat{\boldsymbol{u}}_e$	Unit vector towards Nadir
$\hat{\boldsymbol{W}}_i$	Weight matrix	$\boldsymbol{\Omega}$	Angular velocity matrix
$\boldsymbol{\sigma}_k$	Sigma Point definition	$\boldsymbol{\omega}$	Angular velocity
f	Scalar quantity	$g(A)$	Cost function
$g(\bar{\mathbf{q}})$	Cost function gain	h_ω	Angular momentum
λ_e	Ecliptic Longitude	$\lambda_{\max}$	Scalar quantity
$L(A)$	Loss function	μ	Earth gravitational constant
M	Mean anomaly	n	Matrix Dimension
$\mathbf{c_m}$	Spacecraft center of mass	c_p	Spacecraft center of pressure
$\mathbf{G}_s$	Gravitational Sensitivity Matrix	$\dot{\boldsymbol{\omega}}$	Angular acceleration
$\hat{\mathbf{q}}_k^+$	Estimated quaternion	$\hat{\mathbf{x}}_k^+$	Estimated state vector
$\hat{\mathbf{u}}_e$	Direct Cosine Matrix Unit Vector	$\bar{\mathbf{q}}_{\max}$	Optimal Quaternion
$\mathbf{I_s}$	Spacecraft moment of inertia	$\mathbf{q}$	Quaternion vector
$\bar{\mathbf{A}}_{\text{bias}}$	Bias acceleration vector	$\bar{\boldsymbol{\omega}}_{\text{bias}}$	Bias angular velocity vector
$\bar{\boldsymbol{\omega}}_{\text{gsens}}$	Angular velocity sensitivity vector	$\bar{\boldsymbol{\omega}}_{\text{meas}}$	Measured angular velocity vector
$\bar{\boldsymbol{\omega}}_{\text{SF}}$	Scale factor angular velocity vector	r_{ref}	Reflectance Factor
R_0	Distance from the center of the Earth	u_d	Total disturbance torque
$\boldsymbol{\Omega}$	Angular velocity matrix	ϕ	Solar constant
ψ	Yaw	θ	Pitch

1 Introduction

1.1 Context & Motivation

In 2013, a meteor exploded above the city of Chelyabinsk in Russia, causing significant damage and resulting in numerous injuries. This event highlighted the potential threat posed by larger asteroids in the future. The Asteroid Redirect Mission aims to address this issue, by preventing similar asteroid collisions and mitigate potentially catastrophic events.

Accurate spacecraft attitude determination is crucial for the success of such missions. Gradual attitude drift resulting from system inaccuracies can severely impact trajectory correction manoeuvres. Therefore, the design of a robust attitude determination system is critical. This report introduces a dual-filter design utilising the Unscented Kalman Filter (UKF) and Quaternion Estimator (QUEST) algorithms for spacecraft attitude determination. To achieve the required pointing accuracies, the attitude determination will utilise a suite of sensors including star trackers, sun sensors, Hemispherical Resonator Gyroscopes (HRGs), and Inertial Measurement Units (IMUs). By leveraging data from this sensor suite and considering modelled uncertainties in disturbances, a robust attitude determination system is established, ensuring high performance and accuracy.

1.2 Overview

The report provides an overview of the proposed attitude determination system. It begins by presenting the system design in Section 2, including key requirements, frames of reference, and disturbance modelling. The attitude parameterisation, Section 3, and spacecraft equations of motion, Section 4 are then discussed. Next in Section 5, the system hardware is described, providing an overview of the chosen sensors and system architecture. Sensor models are outlined to further explain their integration in Section 6. Multiple attitude determination algorithms are detailed in Section 7 with the simulations and testing to validate the system design in Section 8. Lastly, the report concludes with final remarks and suggestions for future improvements in Section 9.

2 System Design

2.1 Operation Modes & Performance Requirements

The spacecraft operates in different modes during the mission, including the nominal mode, safe mode, attitude acquisition mode, and stand-by mode. The nominal mode enables telemetry tracking with the transponder activated. Safe mode is used for spacecraft stabilisation, utilising the Reaction Control System (RCS). The attitude acquisition mode ensures minimal pointing error after orbit injection or trajectory correction maneuvers, as defined in Figure 2, taking into account pointing error (PE) as defined by the sum of the system measurement error (ME) and control error (CE).

The spacecraft's performance requirements can be classified into fine-pointing attitude mode and coarse attitude pointing mode. The fine-pointing mode, crucial for trajectory orbit insertion and on-station communication, demands a pointing accuracy of less than 0.1°; this requires star trackers and HRG's. The coarse-pointing mode, which includes instrument initialization, calibration, and unloading of saturated reaction wheels using thrusters, allows larger angle maneuvers before transitioning to the nominal target attitudes. This mode requires a pointing accuracy of 1° which can be met with sun sensors and IMU measurements only. The provided pointing accuracies are an estimation for the initial attitude determination system design provided by Space Mission Engineering, The New SMAD [1].

2.2 Spacecraft Frame of References

To model the spacecraft it is important to keep track of which reference frame is used. The three main frames of reference used for the spacecraft attitude determination are: the inertial frame (X_I, Y_I, Z_I), the orbit reference frame (X_R, Y_R, Z_R) and the spacecraft body frame (X_B, Y_B, Z_B) as shown in Figure 1. The inertial frame serves as a reference for the absolute positioning and motion. The orbit reference frame is a local reference frame fixed to the orbit of the spacecraft, centred at the centre of mass of the Earth and aligned with the orbital plane of the spacecraft. Finally, the satellite body frame is a coordinate system fixed to the spacecraft's body and is used to describe the spacecraft's attitude given by Euler angles: roll, pitch and yaw, (ϕ,θ,ψ).

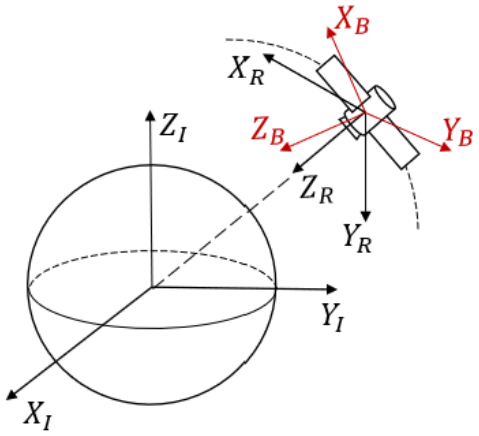

Figure 1: Spacecraft frames of reference.

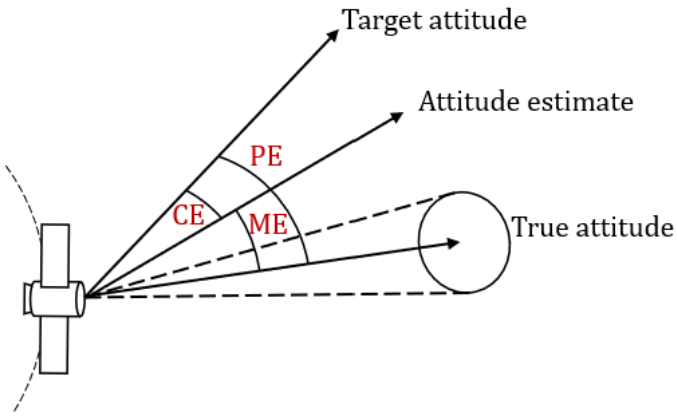

Figure 2: Pointing accuracy definitions.

2.3 Disturbance Model

The environment the spacecraft will operate in affects the attitude estimation process as environment disturbances and mechanical system perturbations produce external and internal torques that act on the spacecraft. These can have a significant impact on the nominal attitude of the spacecraft if not accounted for, therefore, the largest disturbances are quantified in this section.

2.3.1 Gravity Gradient Torque

The gravity gradient torque is exerted on an object in space due to variations in the gravitational field strength; when the spacecraft with a non-uniform mass distribution experiences a gradient in the gravitational field as it orbits Earth. Equation 1 is used to quantify this disturbance torque.

$$\mathbf{u}_{\text{gg}} = \frac{3\mu}{R_0^3}\left[\hat{\mathbf{u}}_{\mathbf{e}} \times (\mathbf{I}_{\mathbf{s}} \cdot \hat{\mathbf{u}}_{\mathbf{e}})\right] \tag{1}$$

The gravity gradient torque, $\mathbf{u}_{\text{gg}}$ is calculated at the parking orbit from the centre of the Earth R_0 [2]. The unit vector towards Nadir, $\hat{\mathbf{u}}_{\mathbf{e}}$, from the spacecraft's centre of mass is used with the spacecraft's moment of inertia, $\mathbf{I}_{\mathbf{s}}$ to quantify the disturbance, where the moment of inertia was assumed to be fixed and non-varying [3].

2.3.2 Solar Radiation Pressure Torque

Solar Radiation Pressure (SRP) torque is the other major external disturbance and refers to the mechanical pressure exerted on the spacecraft due to the exchange of momentum between the spacecraft and the electromagnetic radiation from the absorption, reflection and emission of photons from the Sun. The SRP is a cumulative force acting over the mission duration where the force can cause large deviations in spacecraft trajectories and is modelled using Equation 2.

$$\mathbf{u}_{\text{SRP}} = \frac{\phi}{c} A_{\text{s}}(1 + r_{\text{ref}})(\text{c}_{\text{p}} - \text{c}_{\text{m}})\cos(\varphi) \tag{2}$$

In this equation $\mathbf{u}_{\text{SRP}}$ is the solar radiation pressure torque, c is the speed of light, ϕ is the solar constant at the distance from the sun, A_{s} is the surface area exposed to the sun which is provided by ARM03, along with the centre of pressure c_{p} and centre of mass c_{m} [3]. The angle of incidence of the spacecraft isφ and the maximal SRP torque is considered, where $\varphi = 0$.

2.3.3 Total Disturbance

The internal disturbances arise from liquid sloshing, reaction wheel and cooling system vibrations. While further analysis is required to accurately quantify these disturbances an estimate was made for the worst-case, maximal internal torque disturbances. The total disturbance can, therefore, be quantified by Equation 3.

$$u_d = u_{\text{gg}} + u_{\text{SRP}} + u_{\text{const}} \tag{3}$$

The total disturbance model is comprised of: the gravity gradient torque u_{gg}, the solar radiation pressure torque u_{SRP} and $u_{\text{const}} = 10 * u_{\text{SRP}}$. The term u_{const} term is a constant torque that is considered in the disturbance model to account for the internal disturbances and for unmodelled disturbances, this includes the magnetic field disturbance which was assumed to be small since the spacecraft parking orbit is beyond the range of the Earth's magnetic field to have a significant influence on the spacecraft [4].

3 Attitude Parameterisation

Quaternion attitude representation is widely used for spacecraft attitude determination algorithms as they provide a compact representation of attitude compared to other parameters such as Euler angles, with only four parameters as shown in equation 4. Quaternions also, inherently avoid singularities, such as gimbal lock as the direct cosine matrix is used [5],[6]. An important characteristic for the quaternion is the unit norm which is a condition that must be enforced to avoid distortions or inconsistencies in representing attitude.

$$\mathbf{q} = q_1 i + q_2 j + q_k k + q_4 \tag{4}$$

While the quaternion parameter was primarily used Generalised Rodrigues Parameters (GRPs) are an alternative parameter that is used for quaternion error propagation [7]. Equation 5 defines the relationship between the GRPs and the quaternion, where a is a scalar parameter ranging from 0 to 1, and f denotes an applied scale factor [19]. Another useful quaternion parameter is the Gibbs vector, this is a three element vector that can be formed using Equation 5 evaluated at $a = 0$ and $f = 1$. The Gibbs vector eliminates the need for the scalar component of a quaternion, reducing computational complexity and memory requirements.

$$\mathbf{p} = f \frac{\mathbf{q}}{q_4 + a} \tag{5}$$

4 Spacecraft Equations of Motion

The spacecraft's rotational motion kinematics and dynamics were modelled including the reaction wheels which are a part of the designed reaction control system [9]. Equation 6 describes the mathematical differential equation imposed for the spacecraft attitude dynamics expressed in the spacecraft body frame.

$$\dot{\omega} = -\mathbf{I}_s^{-1}[(\omega \times \mathbf{I_s}\omega) + \omega \times \mathbf{h}_\omega + \dot{\mathbf{h}}_\omega - \mathbf{u}_d] \tag{6}$$

In Equation 6 $\mathbf{h}_\omega$, $\dot{\mathbf{h}}_\omega$ denote the reaction wheel angular momentum and its rate of change respectively. The principal moment of inertia matrix is given by $\mathbf{I_s}$. In this equation there is the addition of the total modelled disturbance torques are shown by $\mathbf{u}_d$ refer back to Section 2.3.

The dynamics are calculated using equation 7, where $[\omega_1,\ \omega_1,\ \omega_1]$ is the spacecraft angular velocity measurement vector, $\boldsymbol{\omega}$, and $\mathbf{q}$ is the quaternion vector, $[q_1,\ q_2,\ q_3,\ q_4]$. The $\mathbf{\Omega}$ term

represents the quaternion skew-symmetric matrix, used in quaternion kinematics to compute the derivative of a quaternion q with respect to time.

$$\dot{\mathbf{q}} = \frac{1}{2}\mathbf{\Omega q} \equiv \frac{1}{2}\begin{bmatrix} 0 & \omega_3 & -\omega_2 & \omega_1 \\ -\omega_3 & 0 & \omega_1 & \omega_2 \\ \omega_2 & -\omega_1 & 0 & \omega_3 \\ -\omega_1 & -\omega_2 & -\omega_3 & 0 \end{bmatrix} \mathbf{q} \tag{7}$$

The Gibbs vector representation is used in Equation 8 and 9. This splits the quaternion into the representation of the axes of rotation and the magnitude of the rotation angle, based on the Gibbs triangular quaternion. These equations were implemented to enforce the unit quaternion norm constraint.

$$\dot{\mathbf{g}} = -\frac{1}{2}\boldsymbol{\omega} \times \mathbf{g} + \frac{1}{2}q_4\boldsymbol{\omega} \tag{8}$$

$$\dot{q}_4 = -\frac{1}{2}\boldsymbol{\omega}^T\mathbf{g} \tag{9}$$

5 System Hardware

The system hardware consists of the necessary onboard sensors, actuators and cold-gas thrusters required for the Attitude Determination & Control System (ADCS), the overall system architecture is shown in Figure 3. The selection process began by analysing the system performance requirements with the main objective to be able to achieve the desired fine pointing accuracy and minimise attitude error. To achieve this all hardware used extensively in space flights were considered and have a certified Technology Readiness Level (TRL) of 9 [10]. A comprehensive trade-off study was performed to select the necessary sensors to use. Several factors were taken into consideration including: mass, cost, size, level of radiation hardening, lifetime, power consumption, accuracy and data rate. These characteristics were weighted accordingly by identifying the importance of each characteristic to achieve the system requirements. This systematic approach was used to create evaluation matrices to quantify the overall performance of each sensor. This enabled the sensors to be ranked and selected based on their suitability to meet the mission performance requirements outlined in Section 2. Additional metrics were included for each specific sensor. For the sun sensors and star trackers, the field of view (FOV), response time were included and for gyroscopes, metrics such as angular rate range and bias stability were used to assess performance. From the sensor options, the final sensors selected to use for the spacecraft are shown in Table 1.

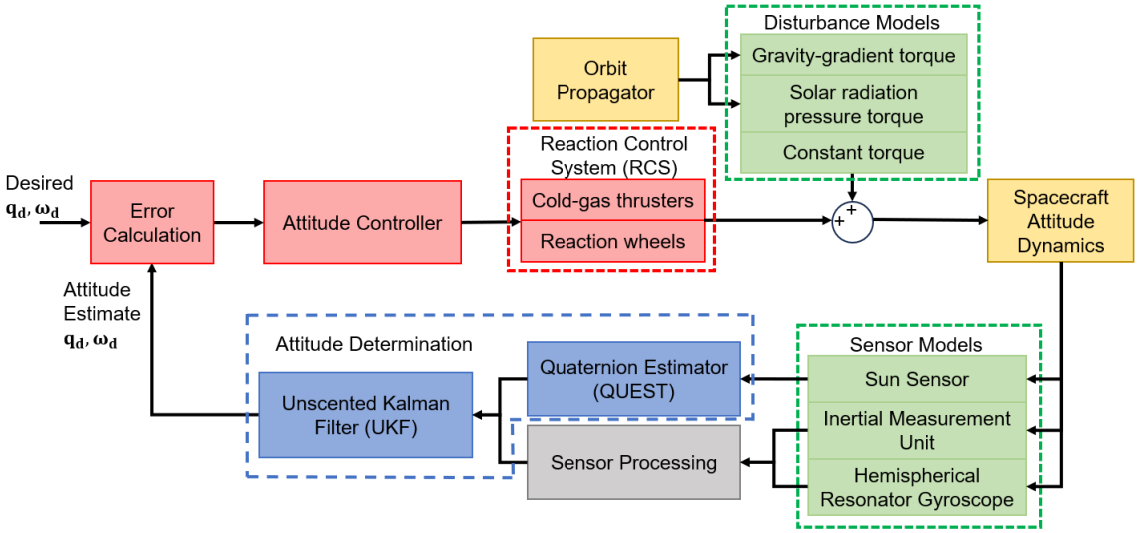

Figure 3: Overview of Attitude Determination system design.

5.1 Redundancy Architecture

The sensor architecture serves a crucial safeguard which enables the ACDS to mitigate potential sensor failures and malfunctions. Multiple sensors were incorporated into the system design with the quantity for each sensor shown in Table 1. This ensures that in the event of a single sensor failure, the spacecraft can continue to gather crucial data for attitude determination and spacecraft operation. The system uses a triple modular redundancy architecture. To achieve this redundancy level there are: 3 star trackers, 3 inertial measurement units and 3 sets of sun sensors, each set consists of 2 sun sensors positioned strategically across the spacecraft to ensure coverage to optimise for sun direction measurements. The gyroscope unit has 4 gyros arranged in an pyramid configuration, adopting an N+1 redundancy structure as this enables for full operation even with a single gyro failure [11].

Table 1: Sensor Hardware Selection

Sensor	Star Tracker: Ball Aerospace CT-2020	Sun Sensor: Solar MEMS Technologies Nano-ISS	Gyroscope Unit: Northrop Grumman Scalable SIRU	Inertial Measurement Unit: Northrop Grumman LN-200S
Accuracy (1σ)	1.5 arcsec	2.0 arcsec	0.0015 °/hr	0.07 °/hr
Power (W)	8	3	23	12
Mass (kg)	3.0	0.005	7.1	0.8
Temperature (°C)	-40 to 85	-40 to 85	-55 to 85	-54 to 71
Sample Rate (Hz)	10	5	100 - 1000	$100 - 1000$
Quantity	3	6	1	3

6 Sensor Modelling

To design the attitude determination system an accurate representation of the measurements provided by the sensors is required. This is achieved using governing equations to attain sun vector measurements, gyroscope angular rates and inertial measurement accelerations. Magnetometer readings were not included due to the defined parking orbit which is beyond the Earth's magnetosphere influence.

6.1 Sun Sensors

The sun sensor measurement can be modelled using geometric relationships between the spacecraft sensor and the Sun. The sun sensor measurement relates the measured intensity to the angle between the sensor's boresight vector and the vector pointing towards the Sun [12]. The sun vector in the inertial frame, $\hat{\mathbf{s}}_i$ can be calculated from the sun sensor model using orbital mechanics involving the mean longitude λ_{mean}, the mean anomaly M, the ecliptic longitude λ_e and obliquity of the elliptic which is 23.44° [13]. The inertial vector shown in Equation 10, can then be converted to the spacecraft body frame to solve for the spacecraft attitudes. To account for uncertainties in sun vector measurements, white Gaussian sensor noise is added to the sun sensor model.

$$\hat{\mathbf{s}}_i = \begin{bmatrix} cos(\lambda_e) \\ cos(e)sin(\lambda_e) \\ sin(e)sin(\lambda_e) \end{bmatrix} \tag{10}$$

6.2 Hemispherical Resonator Gyroscopes

The HRG's selected in Table 1 were modelled using Equations 11 and 12. Where $\bar{\boldsymbol{\omega}}_{\text{meas}}$ are the measured body angular rates, $\bar{\boldsymbol{\omega}}_{\text{b}}$ are the gyroscope body angular rates, $\bar{\boldsymbol{\omega}}_{\text{SF}}$ is a matrix of scaling

factors and misalignment terms. $\mathbf{G}_s$ is the gravitational field strength exerted on the gyroscope and $\bar{\boldsymbol{\omega}}_{\text{gsens}}$ is the corresponding gravitational field strength sensitivity bias. The gyroscope bias and noise components are β, η_v and η_u, where the latter two parameters are Gaussian white noise, which are quantified by the Scalable Siru HRG datasheet, the values are summarised Table 2.

$$\bar{\boldsymbol{\omega}}_{\text{meas}} = \bar{\boldsymbol{\omega}}_{\text{b}} \times \bar{\boldsymbol{\omega}}_{\text{SF}} + \mathbf{G}_s \times \bar{\boldsymbol{\omega}}_{\text{gsens}} + \bar{\boldsymbol{\omega}}_{\text{bias}} + \eta_v \tag{11}$$

$$\dot{\bar{\boldsymbol{\omega}}}_{\text{bias}} = \eta_u \tag{12}$$

Table 2: Northrop Grumman HRG's Scalable SIRU Noise Parameters [14]

Gyro Noise	Value	Unit
Bias Stability	0.0015	°/hr
Noise Equivalent Angle	3	arcsec
Angle Random Walk	0.00015	$^\circ/\sqrt{\text{hr}}$
Angle White Noise	0.003	$\text{arcsec}/\sqrt{\text{Hz}}$

6.3 Inertial Measurement Unit

The gyroscope components in the IMU are modelled as discussed in Section 6.2 and the accelerometers are modelled using Equation 13. In this equation, $\bar{\bar{\mathbf{A}}}_{\text{meas}}$ represents the measured acceleration, $\bar{\bar{\mathbf{A}}}_{\text{imeas}}$ is the inertial measurement unit (IMU) acceleration, $\bar{\bar{\mathbf{A}}}_{\text{SF}}$ is a matrix of scaling factors and misalignment terms, $\bar{\bar{\mathbf{A}}}_{\text{bias}}$ is the accelerometer bias acceleration, and η_v is the IMU measurement noise.

$$\bar{\mathbf{A}}_{\text{meas}} = \bar{\mathbf{A}}_{\text{imeas}} \times \bar{\mathbf{A}}_{\text{SF}} + \bar{\mathbf{A}}_{\text{bias}} + \eta_v \tag{13}$$

7 Attitude Determination Algorithms

7.1 Quaternion Estimator

The QUEST algorithm is an implementation of Davenport's Q-method which offers a least-squares solution to Wahba's problem. This is achieved by minimising the difference between measured vector observations and corresponding vector observations as shown by Equation 14. In Equation 14 $\mathbf{A}$ is an orthogonal matrix that minimises the loss function, $\hat{\mathbf{V}}_i$ are the reference vectors, $\hat{\mathbf{W}}_i$ are the observation vectors and a_i is a set of positively defined weights [15]. Unlike the TRIAD method, which assumes perfect estimates of reference vectors, QUEST accounts for noise and errors present in sensor measurements from sun sensors and star trackers.

$$L(A) = \frac{1}{2}\sum_{i=1}^{n} a_i \left\| \hat{\mathbf{W}}_i - \mathbf{A}\hat{\mathbf{V}}_i \right\|^2 \tag{14}$$

Using an initial estimate the loss function can be evaluated when the gain function, defined by equation 15, is at its maximum; this relates the vector observations in the reference frame to the predicted vector observations in the spacecraft body frame. The gain equation is then re-defined using the attitude profile matrix defined in Equation 16.

$$g(A) = \sum_{i=1}^{n} a_i \hat{\mathbf{W}}_i^T \mathbf{A} \hat{\mathbf{V}}_i \tag{15}$$

$$\mathbf{B} = \sum_{i=1}^{n} a_i \hat{\mathbf{W}}_i^T \hat{\mathbf{V}}_i \tag{16}$$

To simplify the gain function, the quaternion parametrisation is introduced, where Equation 17 represents the gain function in terms of quaternions. The 4×4 $\mathbf{K}$ matrix is used to redefine the gain function using the attitude profile matrix and the trace of $\mathbf{B}$, Equation 18.

$$g(\bar{\mathbf{q}}) = \bar{\mathbf{q}}^T \mathbf{K} \bar{\mathbf{q}} \tag{17}$$

$$\sigma = \text{tr}(\mathbf{B}) \tag{18}$$

$$\mathbf{K} = \begin{bmatrix} \mathbf{B} + \mathbf{B}^T - \sigma\mathbf{I} & \sum_{i=1}^{n} a_i(\hat{\mathbf{W}}_i \times \hat{\mathbf{V}}_i) \\ \sum_{i=1}^{n} a_i(\hat{\mathbf{W}}_i \times \hat{\mathbf{V}}_i) & \sigma \end{bmatrix} \tag{19}$$

The gain function is further modified by introducing Lagrange multipliers to attain the desired formula, Equation 20, to solve for the optimal quaternion $\bar{\mathbf{q}}_{\text{opt}}$ [15]. For this equation the optimisation involves eigenvalue decomposition where the maximum eigenvalue $\lambda_{\max}$ corresponds to the optimal quaternion $\bar{q}_{\max}$. Where $\bar{q}_{\max}$ minimises the difference between the measured and predicted vector observations. The quaternion is then normalised to satisfy the unit norm constraint discussed in Section 3.

$$\mathbf{K}\bar{\mathbf{q}}_{\text{opt}} = \lambda_{\max}\bar{\mathbf{q}}_{\text{opt}} \tag{20}$$

7.2 Extended Kalman Filter

The Extended Kalman Filter (EKF) is an adaption of the linear Kalman Filter (KF) that allows for estimation of the state of a nonlinear system using noisy measurements. It addresses the nonlinearities by linearising the dynamics using a first-order Taylor series expansion about the current estimate and uses a time update and measurement update to estimate the state, the EKF algorithm is outlined in Figure 4.

In the time update step the EKF uses the state vector $\mathbf{x} = [\mathbf{q}, \boldsymbol{\omega}]^T$ and an input control $\mathbf{u} = \mathbf{T_C}$, which is the control torque from the designed the Reaction Control System. The nonlinear system includes the state process noise $\mathbf{w}_k \sim \mathcal{N}(0, \mathbf{Q})$ where $\mathbf{Q}$) is the covariance matrix and is propagated forward with the state vector. In the measurement update step, the EKF uses sensor models to obtain a measured state vector $\mathbf{z} = [\mathbf{q}_{\text{meas}}, \boldsymbol{\omega}_{\text{meas}}]^T$. Using this the optimal Kalman gain is computed, which is used to update the state estimate based on the measurement model where $\mathbf{v}_k \sim \mathcal{N}(0, \mathbf{R})$ is the measurement noise with covariance $\mathbf{R}$ [16].

The error covariance matrix $\mathbf{P}$ quantifies the error between the estimated state $\hat{\mathbf{x}}$ and the real state $\mathbf{x}$. $\mathbf{P}$ is propagated forward using the state transition matrix,$\Phi(\Delta t)$, which approximates the change of state at the current times step [17]. The prediction of the state can be obtained using a numerical integration scheme such as Runge-Kutta.

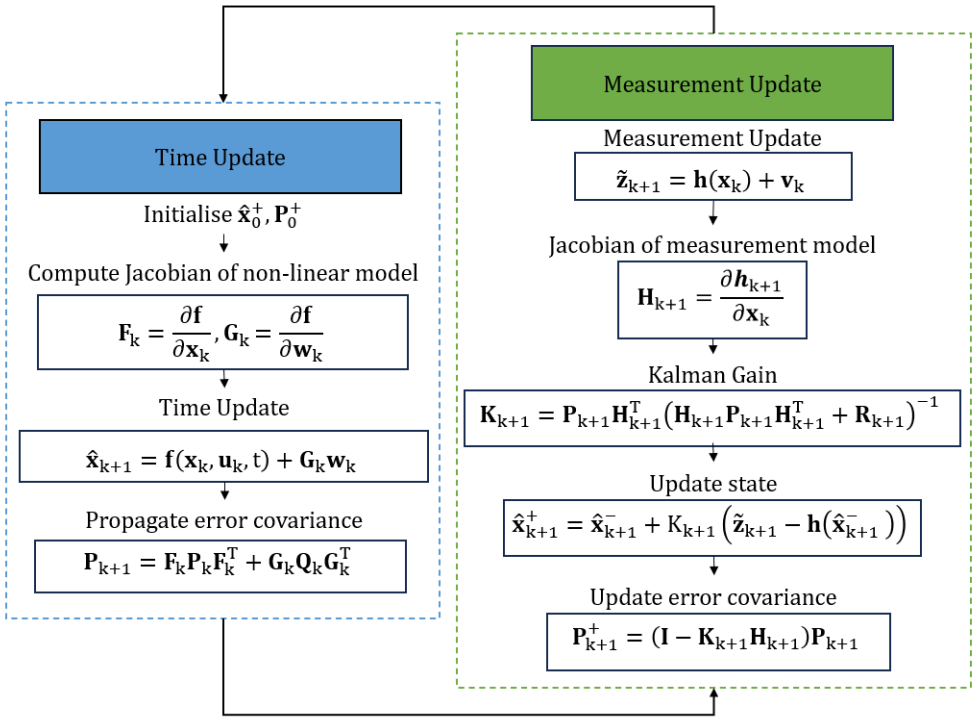

Figure 4: Flow Diagram for the Extended Kalman Filter process.

7.3 Multiplicative Extended Kalman Filter

While the EKF linearises the system dynamics, the Multiplicative Extended Kalman Filter directly operates on the quaternion representation of attitude, utilising quaternion kinematics to propagate and update the attitude estimate. It avoids the linearisation errors associated with the EKF to provide a more accurate estimation of the spacecraft's attitude.

The MEKF updates the quaternion state estimate by applying an incremental quaternion update Equation 21.Where $\bar{\mathbf{q}}$ is the updated true attitude, quaternion state estimate, $\boldsymbol{\delta}\bar{\mathbf{q}}(\mathbf{a})$ represents the incremental quaternion update based on the sensor measurements vector $\mathbf{a}$, and $\bar{\mathbf{q}}_{ref}$ is the reference unit quaternion [18]. The update ensures that the estimated quaternion represents the current attitude relative to the reference orientation.

$$\bar{\mathbf{q}} = \boldsymbol{\delta}\bar{\mathbf{q}}(\mathbf{a}) \otimes \bar{\mathbf{q}}_{ref} \tag{21}$$

7.4 Unscented Kalman Filter

The Unscented Kalman Filter (UKF) is an adaption and extension of the EKF algorithm and addresses the issue of propagating non-linear functions with an identical approach the MEKF imposes. The UKF uses multiple points, instead of a singular points, from which an approximation is made from. These are called sigma points and are points on the Gaussian distribution that are passed through the new non-linear function. Once passed through new mean and variance are calculated for the transformed Gaussian. While it is difficult to transform an entire distribution through a non-linear function it is easier to transform the sigma points which represent the whole distribution.

The sigma points are computed using Equation 22 as defined in Crasidis and Markley's paper on Unscented Filtering [19], where the mathematical rigor of the UKF is presented in detail. Where $\bar{P}_k^+$ and $\bar{Q}_k$ are the respective state and measurement covariance matrices for the estimated state, $\hat{\mathbf{x}}_k^+$. The parameter n is the dimensions of the covariance P and λ is the scaling factor used to determine how far from the mean the sigma points should be chosen and this is given by $\lambda = 3 - n$ for high dimensional systems. The state vector $\mathbf{x} = [\mathbf{q}, \boldsymbol{\omega}]^T$, has an n dimension of 7 due to the seven states.

$$\boldsymbol{\sigma}_k \leftarrow 2n \text{ columns from} \sqrt{(n+\lambda)[P_k^+ + \bar{Q}_k]} \tag{22}$$

The sigma points computed are used to define the sigma point matrix $\boldsymbol{\chi}_k^{(i)}$, given by Equation 23, where every column denotes a set of sigma points, the size of the matrix is determined by the number of dimensions n.

$$\boldsymbol{\chi}_k^{(i)} = \boldsymbol{\sigma}_k^{(i)} + \hat{\mathbf{x}}_k^+ \tag{23}$$

After finding the sigma point matrix, $\boldsymbol{\chi}_k^{(i)}$, it can be used to propagate the state through the non-linear function. For attitude determination, the Generalised Rodrigues Parameters (GRPs) are used to update the quaternion representation where $\boldsymbol{\delta}\hat{\boldsymbol{p}}_k$ denotes the GRPs error defined in 3. The sigma point matrix is updated accordingly resulting in the reduction of the covariance matrix size to be 6×6, as shown by Equation 24. The number of sigma points generated is $2n$ where i is the matrix index defined as $i = 0, 1..12$.The term $\boldsymbol{\chi}_k(i)^{\delta p}$ refers to the attitude error and $\boldsymbol{\chi}_k(i)^{\delta\omega}$ is the angular velocity from the gyroscope measurements.

$$\boldsymbol{\chi}_k(i) = \begin{bmatrix} \boldsymbol{\chi}_k(i)^{\delta p} \\ \boldsymbol{\chi}_k(i)^{\delta\omega} \end{bmatrix} \tag{24}$$

Similar to the MEKF, a new quaternion is defined by multiplying the current estimate with the error quaternion, as Equation 25 shows. This enables the quaternion error to be propagated using the Generalised Rodrigues Parameters avoiding the linearisation process.

$$\hat{\mathbf{q}}_k^+(i) = \boldsymbol{\delta}\hat{\mathbf{q}}_k^+(i) \otimes \hat{\mathbf{q}}_k^+ \tag{25}$$

The Gibbs vector and the scalar quaternion component presented in Equation 25 can be represented using the inverse transform given by Equation 5. The sigma point matrix as shown in Equation 24 can then be defined as Equation 26

$$\boldsymbol{\delta q}_k^+(i) = [\boldsymbol{\delta g}_k^{+T}(i), \delta q_{4_k}^+(i)]^T \tag{26}$$

The extensive use of Generalised Rodrigues Parameters is key to calculate $\boldsymbol{\chi}_k^{(i)}$ and propagate the quaternion error to estimate the states of the attitude dynamics. Using, Equation 26, the predicted mean and covariance can then be calculated based on the sigma point matrix to propagate the state estimate.

8 System Validation

8.1 Parameter Choices & Initialisation

To effectively compare the QUEST, EKF, MEKF and UKF algorithms, its it crucial to initialise several parameters as convergence time is affected. The initial state plays a significant role in the accuracy and performance of these filters. Particularly for the EKF, where linearisation has been carried out, an initial estimate is important to reach a desired performance. The initial state covariance matrix denoted as $\mathbf{P}_0$ is directly correlated with the choice for the initial state estimate and therefore, it is important to make an appropriate estimation. This can be seen by considering an example of a small $\mathbf{P}_0$ value with a large initial error in the initial state. The resulting Kalman Gain would be small and thus a greater weight is place on the model prediction impacting the overall convergence of the model. Furthermore, the process noise covariance $\mathbf{Q}_0$ and measurement noise $\mathbf{R}_0$ were obtained using the measurement noise random noise detailed in the Sensors Modelling Section 6. These matrices were tuned and adjusted to minimise the error for each respective algorithm and are summarised in Table 3.

In order to test the algorithms and evaluate their performance, certain initial values were set to provide a realistic simulation scenario. The true initial angular velocity $\boldsymbol{\omega}_0 = [0.5, 0.5, 0.5]^T$ (rads/sec) and attitude $\boldsymbol{q}_0 = [1, 0, 0, 0]^T$ were chosen. A Simulink model was built based on the spacecraft equations of motion and implemented the QUEST, EKF, MEKF and UKF attitude algorithms. The aim was to simulate the spacecraft trajectory over time and quantitatively evaluate the performance of each estimation algorithm. The simulation includes all the modelled sensor measurements and the total disturbances, with a run time of 30 seconds and a sample rate $\Delta(t) = 0.01$. The initial state estimate $\hat{\mathbf{x}}_0$ is randomly generated where the Gibbs vector and angular velocity were given the defined ranges: $\hat{\mathbf{g}} \in [0.7, 1] \times [0, 0.1] \times [0, 0.1]$ and $\hat{\mathbf{w}} \in [0.4, 1] \times [0.4, 1] \times [0.4, 0.1]$.

Table 3: Tuned measurement and model noise parameters

Parameters	$\mathbf{Q}_0$	$\mathbf{R}_0$
EKF	$0.015^2 \cdot diag([1,1,1,1,1,1,1])$	$0.1^2 \cdot diag([1,1,1])$
MEKF	$0.008^2 \cdot diag([1,1,1,1,1,1,1])$	$0.1^2 \cdot diag([1,1,1])$
UKF	$0.01^2 \cdot diag([1,1,1,1,1,1,1])$	$0.1^2 \cdot diag([1,1,1])$

8.2 Simulation Results & Analysis

In the results shown in Figure 5 and 6, all the attitude determination algorithms are plotted with the exception of the QUEST algorithm due to its worse performance and thus was excluded

to enable a better comparison for the algorithms with similar performance. Digital low pass filters were used to filter out the sensor noise which can be seen plotted along with the the filter algorithms to enable for a better state estimator comparison.

Based on the results presented in Figure 5 and 6, the averaged results over 20 simulations performed, demonstrate the UKF performs the best among the implemented filters. This is shown as the UKF has the lowest Root Mean Square Error (RMSE) values for all the estimated parameters, for roll (φ), pitch (θ), and yaw (ψ) the values are 0.019°, 0.026°, and 0.032° respectively, refer to table 4. Comparatively, the QUEST algorithm produced the least accurate results compared to the other estimation filters, as the results show table 4. A clear comparison of the attitude errors of these two filters are presented in Figure 7, where the QUEST error can be seen to be an order of magnitude greater than the UKF algorithm.

Moreover, the UKF algorithm is suited for handling the nonlinearities introduced by the modelled spacecraft disturbances determined by the orbit propagator. In contrast, the The EKF did not model these nonlinearities as accurately as the UKF due to its inherent linearisation process. This is evidenced by the results from the MEKF, which outperformed the EKF, as shown by the lower RMSE values in Table 4. The MEKF, like the UKF is designed to handle the nonlinear dynamics by using the multiplicative nature of quaternion representation and exhibits a similar convergence rate to the UKF. This shows that the quaternion error calculation has a clear impact on the accuracy of the results where the RMSE attitude error differs by a factor of 2 between the UKF and EKF.

In summary, based on the simulation results, the UKF algorithm demonstrates the best performance in terms of attitude estimation accuracy, particularly for roll, pitch, and yaw parameters. It effectively handles nonlinear dynamics and is suitable for modelling the spacecraft's disturbance and perturbation environment. The UKF algorithm can be complemented by the QUEST algorithm, which can be used as an initialization and contingency filter for the coarse attitude requirements; this ensures a robust attitude determination system for spacecraft attitude estimation.

Table 4: Averaged RMSE Values for the QUEST, EKF, MEKF and UKF.

	QUEST	EKF	MEKF	UKF
φ (°)	0.45	0.056	0.033	0.019
θ (°)	0.39	0.052	0.045	0.026
ψ (°)	0.56	0.057	0.037	0.022
w_x(rad/s)	$9.24 \cdot 10^{-3}$	$14.49 \cdot 10^{-5}$	$11.4 \cdot 10^{-5}$	$7.98 \cdot 10^{-5}$
w_x(rad/s)	$6.62 \cdot 10^{-3}$	$9.04 \cdot 10^{-5}$	$5.53 \cdot 10^{-5}$	$1.87 \cdot 10^{-5}$
w_y(rad/s)	$8.36 \cdot 10^{-3}$	$12.51 \cdot 10^{-5}$	$7.47 \cdot 10^{-5}$	$4.09 \cdot 10^{-5}$

8.3 UKF Optimisation

The UKF was determined to be the most effective attitude estimator for the given spacecraft scenario and conditions based on the numerical analysis. To further investigate its performance and convergence, another Monte Carlo simulation was conducted by considering different values for a and λ, where both are UKF tuning parameters. The simulation results shown in Table 5 were evaluated by numerically integrating the attitude errors for (φ, θ, ψ), over the duration of the simulations to calculate the RMSE. The average results from the 20 runs are summarised in Table 5, where **0.0296** was the best result obtained representing the lowest total error over the course of the simulation, this was for $\lambda = 1$ and $a = 1$. However, other combination of values yielded good results including $\lambda = 0$ for $a = 0$ and $a = 1$. The significance of these results highlights that as a increases the attitude error increases and that the performance of the UKF is independent of the Generalised Rodrigues Parameters used as long as the parameters a and λ are well defined.

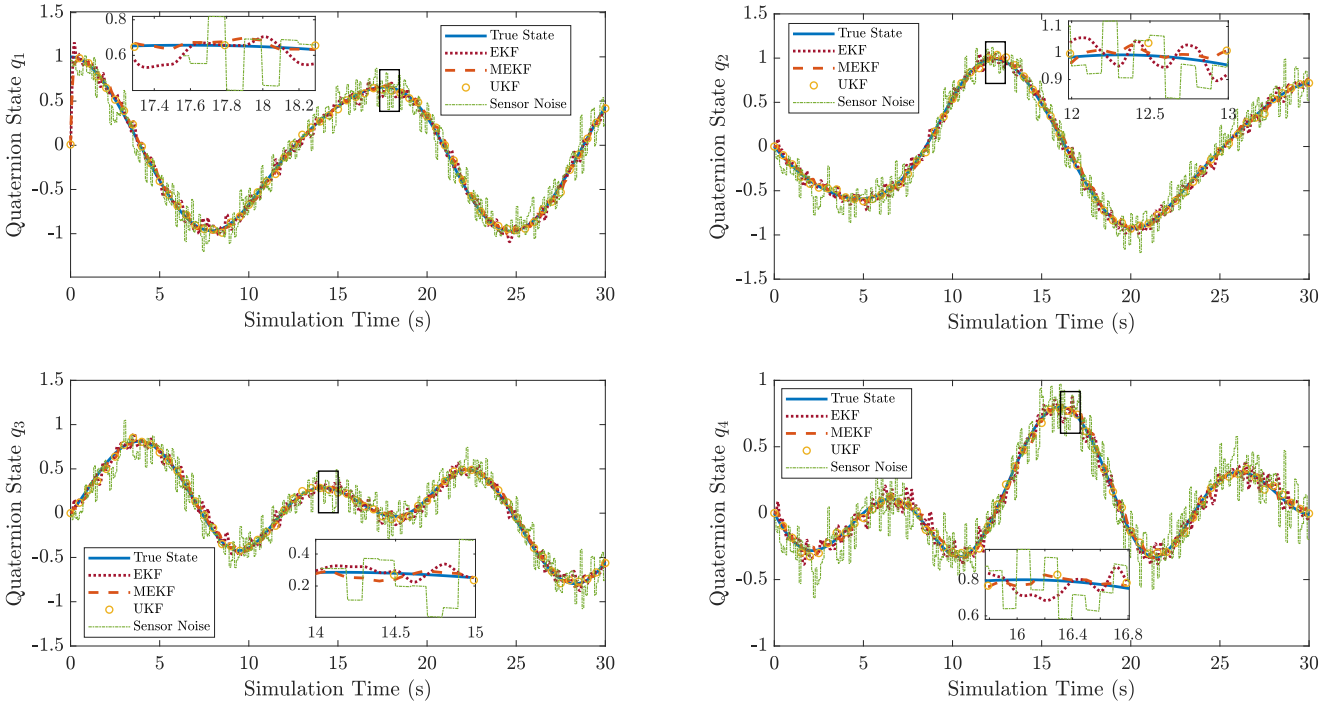

Figure 5: Comparison of Quaternion state estimation plots.

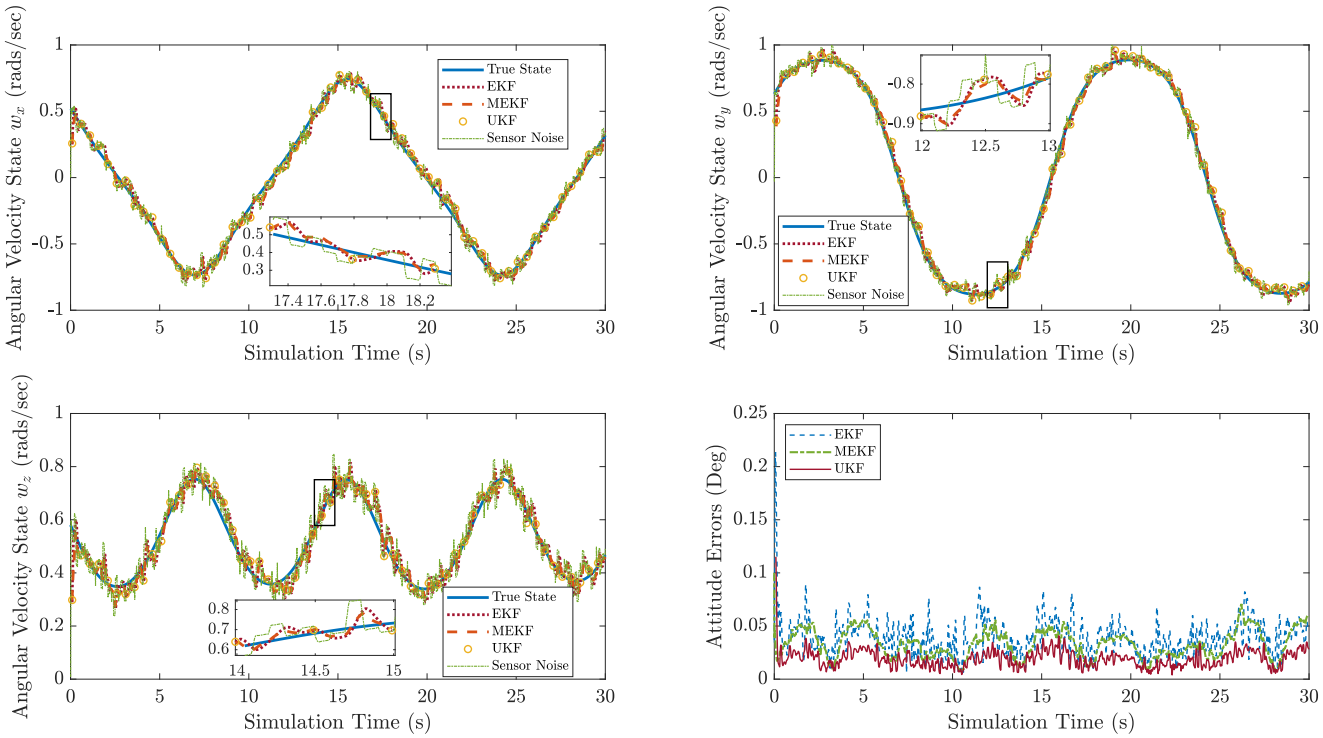

Figure 6: Comparison of the Angular velocity state estimation plots and norm of initial algorithm attitude errors for the EKF, MEKF and UKF.

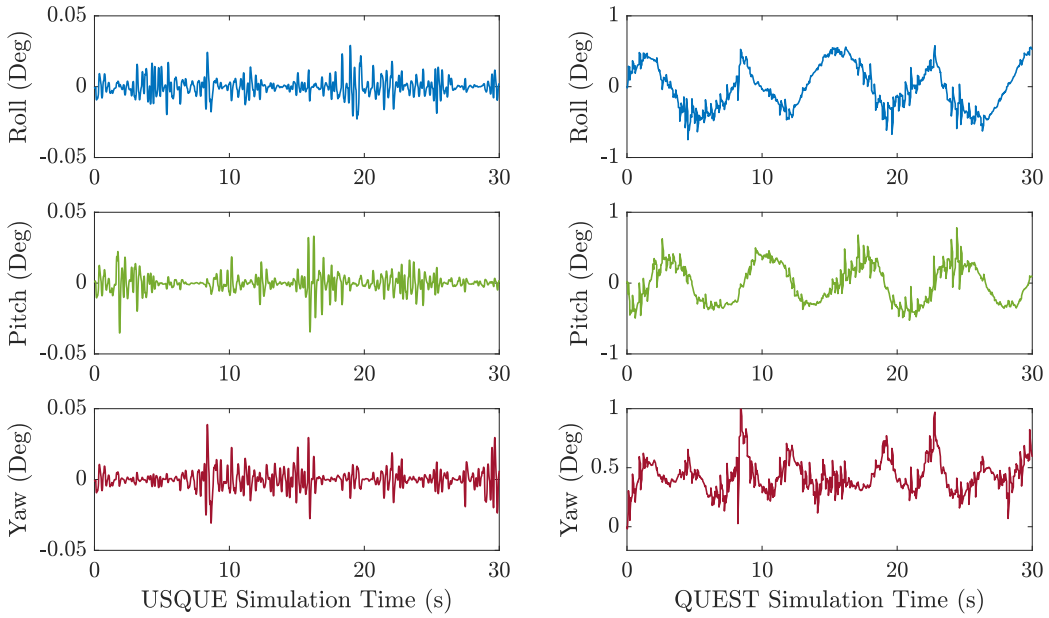

Figure 7: Attitude error plots for the UKF (left) and QUEST algorithms (right).

Table 5: Averaged RMSE Results for UKF Parameter Optimisation

	$a = 0$	$a = 1$	$a = 2$	$a = 3$
$\lambda = -3$	0.129	0.1055	0.0701	0.07004
$\lambda = -2$	0.0673	0.0537	0.0592	0.0586
$\lambda = -1$	0.0418	0.0299	0.0324	0.0329
$\lambda = 0$	0.0331	0.0328	0.0365	0.0468
$\lambda = 1$	0.0395	**0.0296**	0.0672	0.0479
$\lambda = 2$	0.0747	0.0495	0.0422	0.0501
$\lambda = 3$	0.0957	0.0731	0.1163	0.1878

9 Conclusion

This report presents a comprehensive analysis of the attitude determination system for the Asteroid Redirect Mission spacecraft. The primary objective was to design an optimal system that satisfies the requirements of both fine pointing and coarse pointing modes. Disturbance environment quantification and careful selection of sensor hardware were performed using evaluation matrices. Four algorithms (QUEST, EKF, MEKF, UKF) were tested, with the UKF demonstrating superior performance and all algorithms achieving RMSE attitude errors below the required pointing error threshold. The UKF was integrated with the QUEST algorithm to enhance system robustness and serve as an initialization and contingency mechanism. However, further testing is necessary to evaluate the UKF's performance during complex spacecraft maneuvers and verify its effectiveness in mitigating attitude drift. Integrating the state estimator system with suitable digital low-pass filtering in conjunction with the designed attitude controller would ensure a robust and reliable ADCS, with any compatibility issues addressed. Future improvements should focus on conducting rigorous simulations to analyze algorithm convergence in real-time control scenarios, providing valuable insights for refining or adapting the dual-attitude determination system and ensuring its reliability in practical mission scenarios.

References

[1] Wertz, James R., and Wiley J. Larson. *Space Mission Analysis and Design.* 3rd ed., Microcosm Press, 1999.

[2] G. Barbosa Ribeiro ARM02 - Mission Design & Analysis, Concept Exploration, Parking Orbit Definition, and Constellation Design for an Asteroid Redirect Mission, Imperial College London, Department of Aeronautics, 2023.

[3] P. Aaron ARM03 - Spacecraft mechanical design and subsystem integration, Structural Design, Micrometeroid Impact Analysis and Deployable Mechanisms for Project KINEXUS, Imperial College London, Department of Aeronautics, 2023.

[4] S. R. Starin and J. Eterno, Attitude determination and control systems, 2011.

[5] Hemingway, E. G., & O'Reilly, O. M. Perspectives on Euler angle singularities, gimbal lock, and the orthogonality of applied forces and applied moments, *Multibody System Dynamics*, vol. 44, Sep. 15, 2018.

[6] Choukroun, D., Weiss, H., Bar-Itzhack, I. Y., & Oshman, Y. Direction cosine matrix estimation from vector observations using a matrix Kalman filter, *IEEE Transactions on Aerospace and Electronic Systems*, vol. 46, no. 1, Jan. 2010.

[7] Giorgi, Gabriele, Generalized Rodrigues Parameters for Attitude Representation 2019, Available: `https://elib.dlr.de/127011/1/Giorgi_GRPs_archive.pdf`

[8] Crassidis, J. L. and Markley, F. L. Unscented filtering for spacecraft attitude estimation, *Journal of Guidance, Control, and Dynamics*, vol. 26, no. 4, Jul. 2003.

[9] O. Brook, ARM04 - Spacecraft Subsystems, Attitude Controller Design for Asteroid Redirect Mission, Imperial College London, Department of Aeronautics, 2023.

[10] Mankins, J. C. Technology readiness levels, *White Paper*, April, 1995.

[11] Bhatia, D. Attitude determination and control system design of sub-arcsecond pointing spacecraft. J Guid Control Dyn. 2021; Available: `https://doi.org/10.2514/1.G005116`

[12] Liebe, C. C., & Mobasser, S. MEMS based sun sensor, In *2001 IEEE Aerospace Conference Proceedings (Cat. No. 01TH8542)* (Vol. 3, pp. 3-1565). IEEE, Mar. 10, 2001.

[13] Jung, H., & Psiaki, M. L. Tests of magnetometer/sun-sensor orbit determination using flight data, *Journal of Guidance, Control, and Dynamics*, vol. 25, no. 3, May 2002.

[14] Northrop Grumman Corporation, Scalable SIRU Family of Products Brochure, Available: `https://www.northropgrumman.com/what-we-do/air/multifunction-sensors/`

[15] F. L. Markley, J. Crassidis, and Y. Cheng, Nonlinear attitude filtering methods, in *AIAA Guidance, Navigation, and Control Conference and Exhibit*, Aug. 2005

[16] A. Knoll and D. Amato, Spacecraft systems lecture 12 - attitude determination and Control, Jan. 26, 2023.

[17] E. J. Lefferts, F. L. Markley, M. D. Shuster, Kalman filtering for spacecraft attitude estimation, *Journal of Guidance, Control, and Dynamics*, vol. 5, no. 5, Sep. 1982

[18] F. L. Markley, Multiplicative vs. additive filtering for spacecraft attitude determination, *Dynamics and Control of Systems and Structures in Space*, vol. 18, Jul. 2004

[19] Crassidis, J. L., & Markley, F. L. Unscented filtering for spacecraft attitude estimation, *Journal of Guidance, Control, and Dynamics*, vol. 26, no. 4, Jul. 2003.

A Sensor Evaluation Matrices

Table 6: Inertial Measurement Unit Evaluation Matrix

Criteria	Collins Aerospace RAD750 IMU	Honeywell HG1930 IMU	Northrop Grumman LN-200 IMU	Silicon Sensing CRH02 IMU
Mass	Moderate	Light	Moderate	Light
Cost	High	Moderate	High	Low
Dimensions	Compact	Compact	Compact	Compact
Radiation Hardening	High	High	High	Moderate
Lifetime	Long	Moderate	Moderate	Moderate
Power Consumption	Moderate	Low	Moderate	Low
Accuracy	High	High	High	Moderate
Data Rate	Moderate	Moderate	Moderate	Moderate

Table 7: Gyroscope Evaluation Matrix

Criteria	Northrop Grumman Scalable SIRU-ETM	KVH Industries DSP-1750 Fiber Optic Gyro	Safran Electronics & Defense HRG3000 Hemispherical Resonator Gyro	Silicon Sensing CRS03 MEMS Gyro
Mass	Light	Light	Moderate	Light
Cost	High	High	Moderate	Low
Dimensions	Compact	Compact	Compact	Compact
Radiation Hardening	High	Moderate	High	Moderate
Lifetime	Long	Long	Long	Moderate
Power Consumption	Low	Low	Low	Very Low
Accuracy	High	High	High	Moderate
Angular Rate Range	Wide	Wide	Moderate	Wide
Bias Stability	Excellent	Excellent	Moderate	Excellent

Table 8: Sun Sensor Evaluation Matrix

Criteria	Solar MEMS Sun Sensor	Cubesat Sun Sensor	Honeywell HRS-3 Sun Sensor	L-3 ETI Sun Sensor
Mass	Light	Light	Light	Moderate
Cost	High	Low	Moderate	Moderate
Dimensions	Compact	Small	Compact	Compact
Radiation Hardening	High	Moderate	High	Moderate
Lifetime	Long	Moderate	Long	Long
Power Consumption	Low	Moderate	Low	Low
Accuracy	High	Very Low	High	High
Field of view	Wide	Moderate	Wide	Wide
Response Time	Fast	Moderate	Fast	Fast

Table 9: Star Tracker Evaluation Matrix

Criteria	Ball Aerospace High Accuracy Star Tracker (HAST)	Honeywell HI-STAR 100 Star Tracker	Surrey Satellite Technology Ltd SSTL-100	Celestial Systems Limited (CSL) StarTrack-100
Mass	Light	Light	Light	Moderate
Cost	High	Moderate	Low	Moderate
Dimensions	Compact	Compact	Compact	Large
Radiation Hardening	High	High	Moderate	Moderate
Lifetime	Long	Long	Long	Long
Power Consumption	Low	Low	Very Low	Moderate
Accuracy	High	High	Moderate	High
Field of view	Wide	Wide	Moderate	Wide
Attitude Determination	Wide	High	Moderate	High
Data Update Rate	High	Moderate	Moderate	High

B Simulink Model

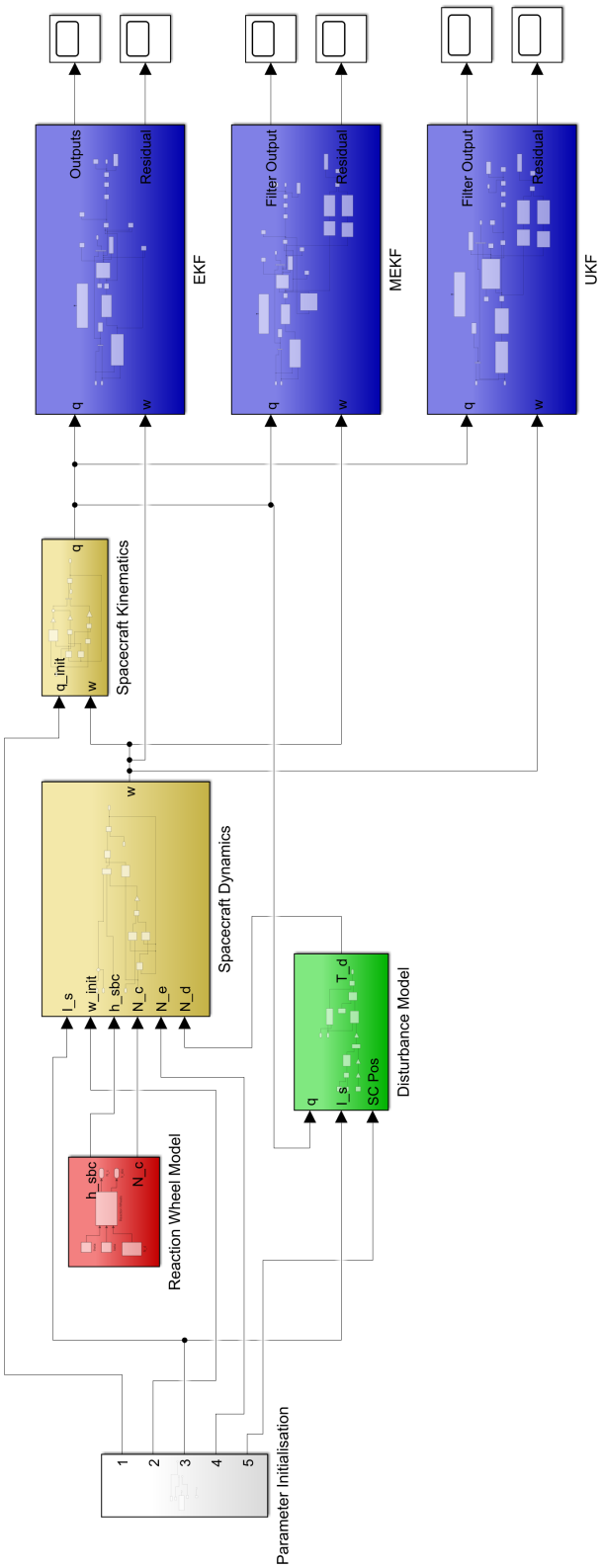

Figure 8: Designed Simulink Model